

Article

Origin of Redbeds in the Neoproterozoic Socheong Formation and Their Relation to the Dashigou Large Igneous Province

Hawon Yun ¹, Seung Hwan Lee ² and Inah Seo ^{1,3,*}

¹ Department of Environment and Energy, Jeonbuk National University, Jeonju 54896, Republic of Korea; yunhawon@jbnu.ac.kr

² Geology and Space Division, Korea Institute of Geoscience and Mineral Resources, Daejeon 34132, Republic of Korea; lsh07@kigam.re.kr

³ Department of Earth and Environmental Sciences, Jeonbuk National University, Jeonju 54896, Republic of Korea

* Correspondence: inahseo@jbnu.ac.kr

Abstract: During the latest Mesoproterozoic–Early Neoproterozoic era, extensional regimes generated a number of sedimentary basins in various regions in the Sino-Korean Craton. Mantle-plume emplacements are widely recognized in the sedimentary strata as mafic dikes and sills of the Dashigou Large Igneous Province (LIP). The occurrence of Fe-rich redbeds is first reported in the Neoproterozoic Socheong Formation of the Sangwon Supergroup in the Pyeongnam Basin. Their geochemical and mineralogical characteristics indicate basin-wide Fe enrichment due to hydrothermal fluid input. The episodic yet repetitive hydrothermal injection into the basin generated short-lived anoxia, recorded as greenish-gray coloration in the ferruginous beds. This hydrothermal fluid was likely sourced from the mafic igneous activities involved in the Dashigou LIP. The redbeds can be utilized as key beds for intra- or inter-basinal stratigraphic correlation and to study the negative carbon isotope excursions that occurred in the genetically related basins in the region (e.g., the Sangwon, Xu-Huai, and Dalian basins).

Keywords: Socheong Formation; Sangwon Supergroup; Neoproterozoic; redbed; Large Igneous Province



Citation: Yun, H.; Lee, S.H.; Seo, I. Origin of Redbeds in the Neoproterozoic Socheong Formation and Their Relation to the Dashigou Large Igneous Province. *Minerals* **2024**, *14*, 59. <https://doi.org/10.3390/min14010059>

Academic Editors: Richard E. Ernst and Hafida El Bilali

Received: 17 November 2023

Revised: 31 December 2023

Accepted: 31 December 2023

Published: 2 January 2024



Copyright: © 2024 by the authors. Licensee MDPI, Basel, Switzerland. This article is an open access article distributed under the terms and conditions of the Creative Commons Attribution (CC BY) license (<https://creativecommons.org/licenses/by/4.0/>).

1. Introduction

During the Late Paleoproterozoic–Neoproterozoic period (1800–541 Ma), an extensional tectonic regime generated multiple rifts in the Sino-Korean Craton (SKC) [1]. A number of sedimentary basins, including the Dalian, Pyeongnam (Pyeongnam), and Xu-Huai basins (Figure 1A), developed simultaneously in the SKC during the Early Neoproterozoic period (ca. 1000–800 Ma). Although these basins were generated by a common rifting system, namely the Xu-Huai Rift System, the sedimentary successions (represented by the Qingbaikou System in North China) in the basins have been studied separately, largely owing to their ambiguous inter-basin relationship (e.g., [1–4]). A few comparative studies have analyzed the geologic affinities between these basins, particularly to analyze their common detrital provenances and contemporaneous igneous activities [5–9]. However, the geological history of the Sangwon Supergroup of the Pyeongnam Basin remains relatively unexplored, owing to the limited geologic information about the region.

The sedimentary strata deposited in these extensional basins, which are affected by the Xu-Huai Rift System, are commonly intruded by mafic sills or dike swarms shared by a common mantle-plume source [4,10]. This plume-related igneous activity is thought to have caused a large mafic extrusion, covering an area of 50,000 km², referred to as the Dashigou Large Igneous Province (LIP) [11–13]. The emplacement of the LIP had dramatic effects on the regional and/or global environment during the Phanerozoic, e.g., warming, cooling, ocean acidification, marine anoxia, and mass extinction [14]. However, the influence of this enormous magmatic activity on the semi-enclosed sedimentary basins

of the Xu-Huai Rift System remains uncertain. Recently, negative carbon isotope excursions (nCIEs) have been identified in the Xu-Huai, Dalian, and Pyeongnam basins, suggested to be the earliest-known nCIE events attributed to the formation of the Dashigou LIP [15–17]. However, their concurrent causation is not well-understood, partly because of the lack of knowledge of the environmental and biotic responses to the emplacement of the LIP.

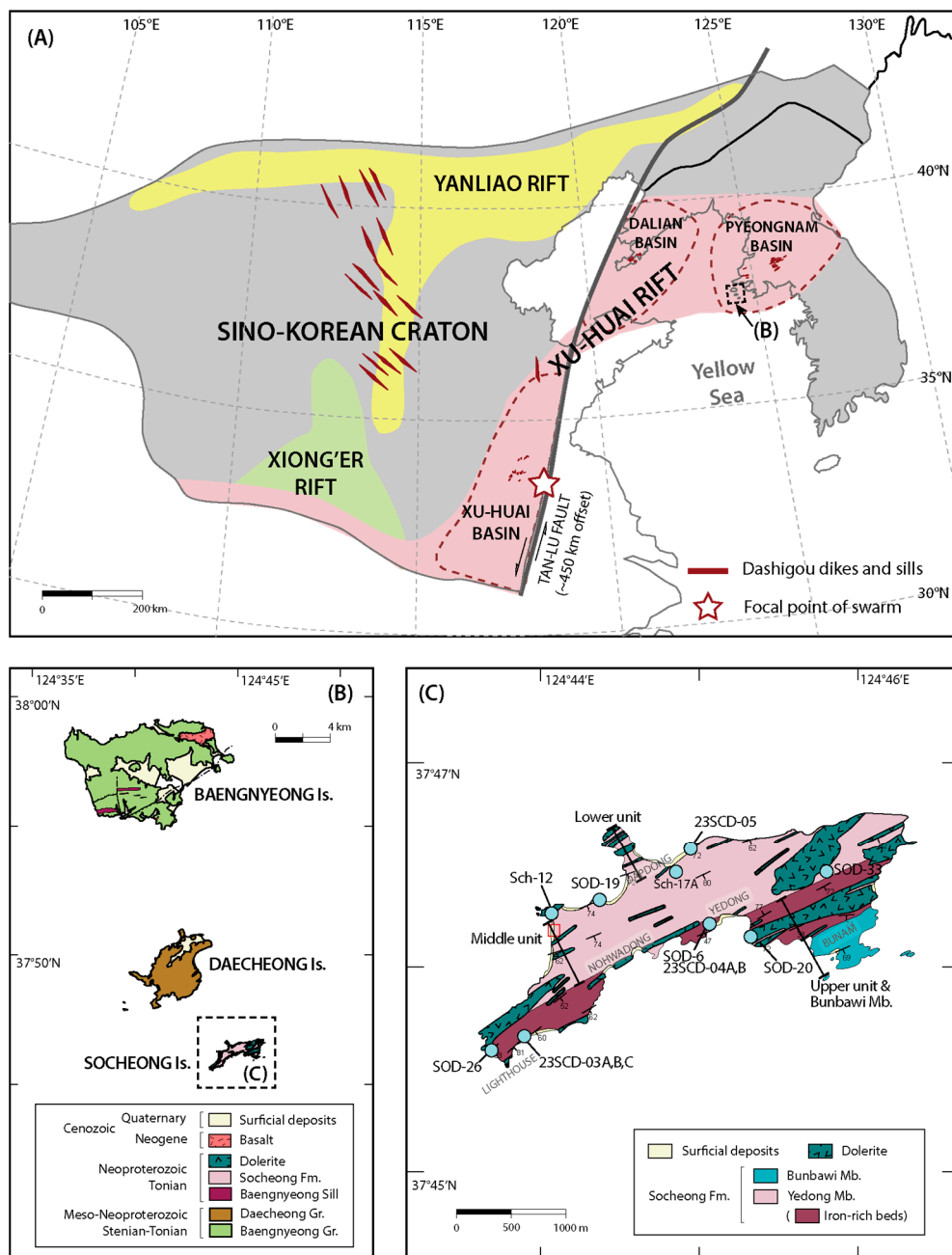


Figure 1. (A) Simplified tectonic map of Sino-Korean Craton, portraying three representative sedimentary basins, namely, the Pyeongnam (Pyeongnam), Dalian, and Xu-Huai basins, during the latest Mesoproterozoic–Early Neoproterozoic period (modified after [4,6,12,18]); also shown are 940–890 Ma Dashigou dike swarms and their focal point (star) to mark the plume center [12]. (B) Simplified geologic map of the Baengnyeong, Daecheong, and Socheong islands (modified after [19]). (C) Geologic map of Socheong Island, presenting the locations of the redbeds and the sampling sites. The locations of representative sections are indicated as solid lines.

In this study, we report the occurrence of redbeds in the Socheong Formation, Socheong Island, South Korea, which is part of the Sangwon Supergroup of the Pyeongnam Basin. The origins of the redbeds and the co-occurring iron-rich greenish beds were determined from their geochemistry and mineralogy, and their relation to the region mafic igneous activity was also assessed. The hydrothermal activity associated with the Dashigou LIP and the relevant mafic igneous activities supplied Fe, while triggering local anoxia in the basin. The results of this study support the existing hypothesis that the formation of the LIP had a great influence on the biosphere and seawater chemistry, even during the Proterozoic [14,20].

2. Geological Settings

The sedimentary strata in the Baengnyeong, Daecheong, and Socheong islands have long been regarded as southwestern extensions of the Sangwon Supergroup in the Pyeongnam Basin in North Korea [21]. The Sangwon Supergroup is a (meta)sedimentary succession that corresponds to the Qingbaikou System (1000–780 Ma) in North China. The Sangwon Supergroup in mainland North Korea is subdivided into the Jikhyeon (Jikyong), Sadangu, Mukcheon (Mukchon), and Myeoraksan (Myoraksan) groups (in stratigraphically ascending order) [22].

Socheong Island is situated in the Yellow Sea, approximately 14 km from Jangsan Cape in South Hwanghae Province of North Korea (Figure 1). Kim and Kim [23] suggested that the sedimentary strata are related to the Mukcheon and Myeoraksan groups of the upper Sangwon Supergroup of North Korea, based on the stromatolite morphotypes discovered on Socheong Island. Lee et al. [24] reported bacterial microfossils as supporting evidence for the Neoproterozoic ages of the stromatolite. However, owing to the wide stratigraphic range of the Precambrian bacterial microfossils, a precise stratigraphic framework could not be established for the Socheong, Daecheong, and Baengnyeong islands.

Precise geological surveying and mapping of the Socheong, Daecheong, and Baengnyeong islands were carried out by Cho et al. [19], who developed a lithostratigraphic framework of the Proterozoic strata of the three islands. The Proterozoic sedimentary strata distributed in the Baengnyeong, Daecheong, and Socheong islands are called the Baengnyeong and Daecheong groups and the Socheong Formation, respectively (Figure 1B). The Baengnyeong and Daecheong groups are subdivided into the Nampori, Junghwadong, and Dumujin formations and the Jiduri and Dokbawi formations, respectively, in ascending stratigraphic order [19]. The Socheong Formation, the only formal lithostratigraphic unit on Socheong Island [19], is subdivided into two members (in ascending stratigraphic order): the Yedong and Bunbawi members (Figures 1C and 2A). The Yedong Member consists mainly of alternating sandstone–siltstone–shale layers, with partially intercalated limestone layers. The Bunbawi Member consists of thick limestone strata, with thin shale layers containing stromatolite fossils from the Neoproterozoic Era [23].

The depositional ages of the Baengnyeong, Daecheong, and Socheong formations were constrained by Cho, Lee, and Park [19], based on the maximum depositional ages of the strata determined by the igneous ages of the detrital zircons within, and the intrusion ages of, the mafic sills. Cho, Lee, and Park [19] reported the detrital zircon U-Pb ages of the Socheong Formation, with the youngest age peak estimated to be 900 Ma (Figure 2B,C). The U-Pb ages of the zircons (884 ± 4 Ma) and baddeleyites (888 ± 5 Ma) of the intruding dolerite (SOD-20 in Figure 2A) indicate that the depositional age of the Socheong Formation is the Tonian Period of the Neoproterozoic Era. Similarly, the depositional ages of the Daecheong and Baengnyeong groups range from 1040 Ma to 940 Ma, corresponding to the Mesoproterozoic (Stenian)–Neoproterozoic (Tonian) period [19].

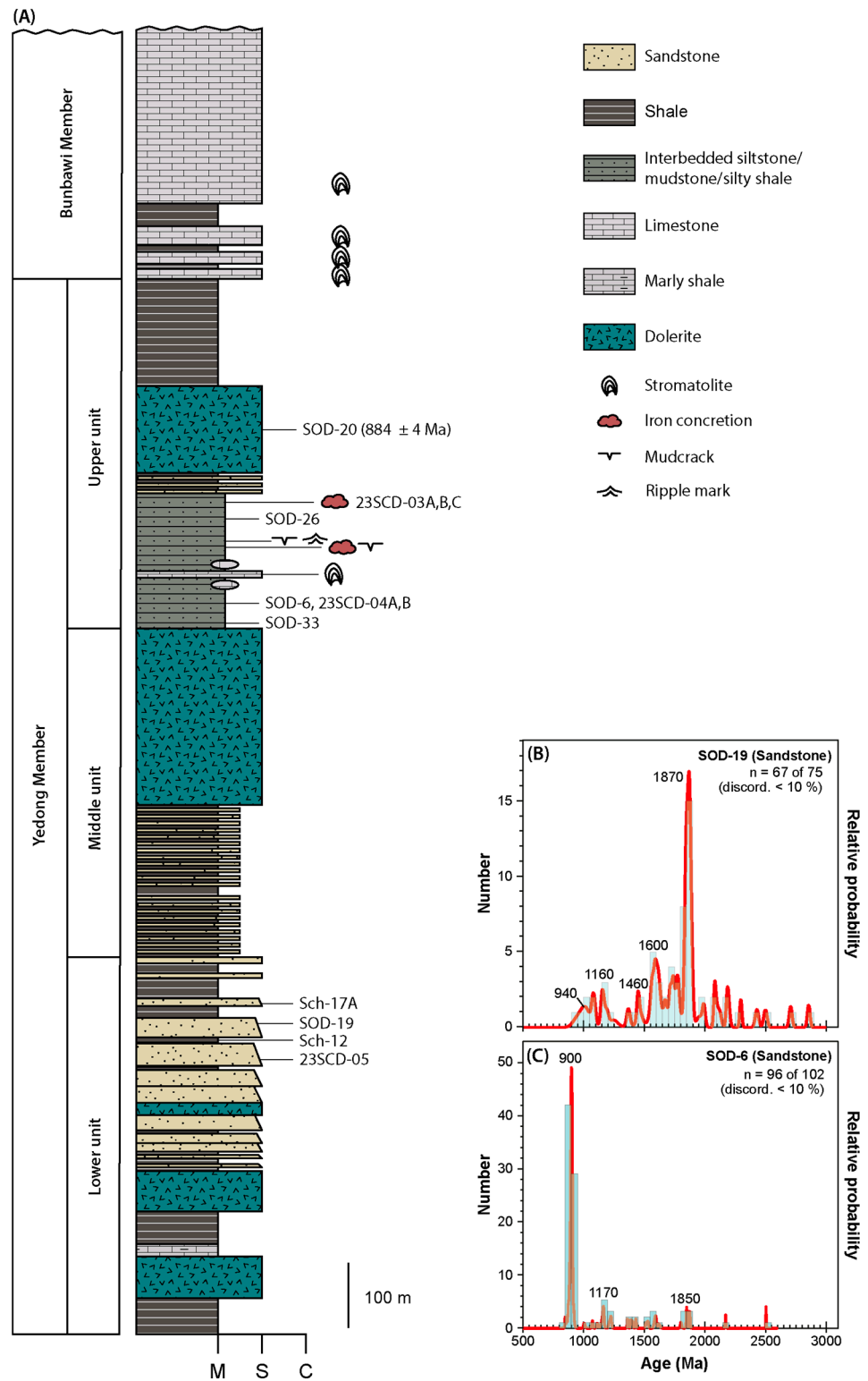


Figure 2. (A) Schematic illustration of the columnar section of Socheong Formation and positions of samples collected. (B,C) LA-MC-ICP-MS U-Pb isotopic analyses results for samples of Socheong Formation (data from [10]).

3. General Lithology of Socheong Formation and Redbed Occurrences

A schematic of the columnar section of the Socheong Formation is shown in Figure 3. The lower part of the Yedong Member is best exposed in the Dapdong area at the northern cape of the island, near the port. The lower part is mainly characterized by fine-grained

gray sandstone intercalated with thin dark gray mudstone (Figure 3A), dark gray shale, and light gray marly shale (Figure 3B,C). The thicknesses of the individual sandstone–mudstone couplets are 2–10 cm, sometimes exceeding several decimeters. The monotonous repetition of fine sandstone with graded bedding overlain by thin mudstone beds and remarkable lateral continuity (>10 m) are typical of low-density turbidite facies (Figure 3D). As shown in the figures, the dark gray shale and light gray marly shale exhibit parallel and laterally continuous laminae, indicating suspension settling. The lower part of the Yedong Member indicates a distal hemipelagic depositional process. Notably, in the Dapdong area, dolerites are frequently found as sills that are parallel to bedding planes.



Figure 3. Outcrop photographs of the representative lithologies of the lower unit of Yedong Member, Socheong Formation. (A) Fine-grained gray sandstone intercalated with thin dark gray mudstone; (B) dark gray shale; (C) light gray marly shale; and (D) intercalated sandstone–mudstone exhibiting remarkable lateral continuity.

The middle part of the Yedong Member was well-exposed along the western coast of the island; a detailed columnar section of this strata has been provided by [19]. It is characterized by thick (>50 cm) bedded sandstone, interbedded mudstone–siltstone, and laminated dark gray shale. The most dominant lithology is interbedded mudstone–siltstone couplets with parallel/horizontal bedding (Figure 4A), occasionally occurring with thick laminated shale (Figure 4B). The outer shelf environment is presumed to be based on the lateral continuity of mudstone–siltstone beds, without any tidal or wave-generated substructures, such as mudstone rip-ups or internal cross-lamination. The intermittent invasion of the coarse-grained sandstone layer may indicate the occurrence of storm events.

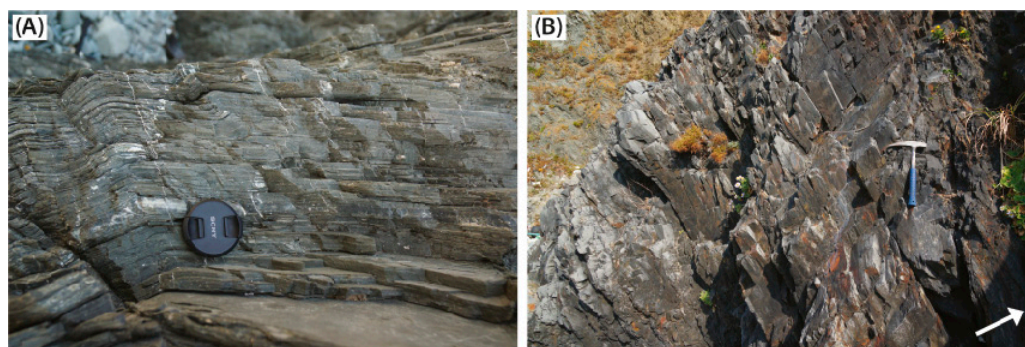


Figure 4. Outcrop photographs of middle unit of Yedong Member, Socheong Formation: (A) interbedded mudstone–siltstone with parallel/horizontal bedding and (B) thick dark gray shale exhibiting parallel bedding.

The upper part of the Yedong Member consists of plane or wavy laminated shale that is occasionally intercalated with tabular or lenticular-shaped limestone (Figure 5A), interbedded mudstone, and siltstone, exhibiting flaser, wavy, and lenticular bedding patterns (Figure 5B), and thick sandstone (Figure 5C). The siltstone–mudstone interbeds are very thin to thin-bedded, with planar to undulated bedding planes, and cross-laminations within the siltstone can be noted. Mudcracks (Figure 5D,E) and symmetrical wave-ripple marks (Figure 5F) were observed on the bedding planes of the mudstone, for which raindrop imprints were reported [25]. These characteristics suggest a tidally influenced marginal marine environment above the wave base, which was occasionally exposed subaerially.

The upper boundary of the Yedong Member is marked by the thick development of a white–grayish-white limestone bed of the Bunbawi Member in the Bunam area (Figure 1C). The limestone in the lower unit exhibits a lenticular or tabular form, generally <1 m in thickness, being intercalated with purple or dark gray shale (Figure 6A), whereas the upper unit is almost entirely composed of stromatolitic limestone (Figure 6B). In the upper unit, the limestones are strongly deformed and partly metamorphosed into marble; thus, their bedforms and internal structures are sometimes amalgamated and thus difficult to discern [26]. Kong and Lee [26] provided a more detailed morphological description of the stromatolites.

The interbedded mudstone–siltstone and laminated shale of the upper Yedong Member exhibited a wide range of colors, including light and dark-gray, purple, red, and greenish-gray. The redbeds occur as ferruginous red-purple shale and interbedded siltstone–mudstone in the upper part of the Yedong Member (Figure 7A,B). They can be traced along the southeastern coast of Socheong Island, from the Deungdae (Socheong Lighthouse) to Yedong ports, and along the boundary between the Yedong and Bunbawi members (Figure 1C). The redbeds are often intercalated with greenish-gray beds that have similar lithologies; in some localities, the color changes from greenish-gray at the base to a reddish color in the upper section (Figure 7C). Some localities that exhibited hydrothermal vein injection were greenish-gray in color, indicating the reducing effect of the hydrothermal fluids (Figure 7D). The Fe concretions (ranging from mm to cm in diameter) were occasionally found in the greenish-gray beds (Figure 7E), but not in the purple-red beds. The purple shale underlying the upper boundary of the Yedong Member (Figure 7F) had thickness of >100 m.



Figure 5. Outcrop photographs of upper unit of Yedong Member, Socheong Formation: (A) Shales with tabular or lenticular limestone; (B) interbedded mudstone and siltstone with wavy beddings; (C) thick sandstone; (D,E) Mudcracks; and (F) wave-ripple marks on the mudstone bedding planes.

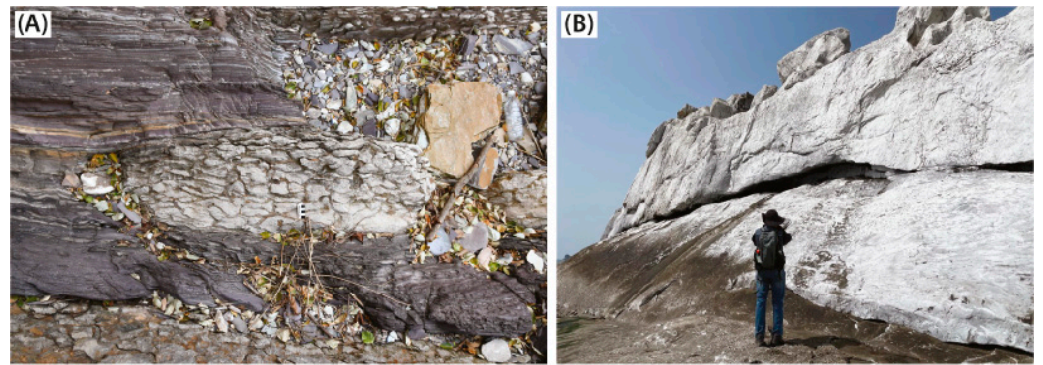


Figure 6. Outcrop photographs of Bunbawi Member of Socheong Formation: (A) lenticular limestone interbedded with purple shale (photo courtesy: Jeong-Hyun Lee) and (B) thick strata of stromatolitic limestone.

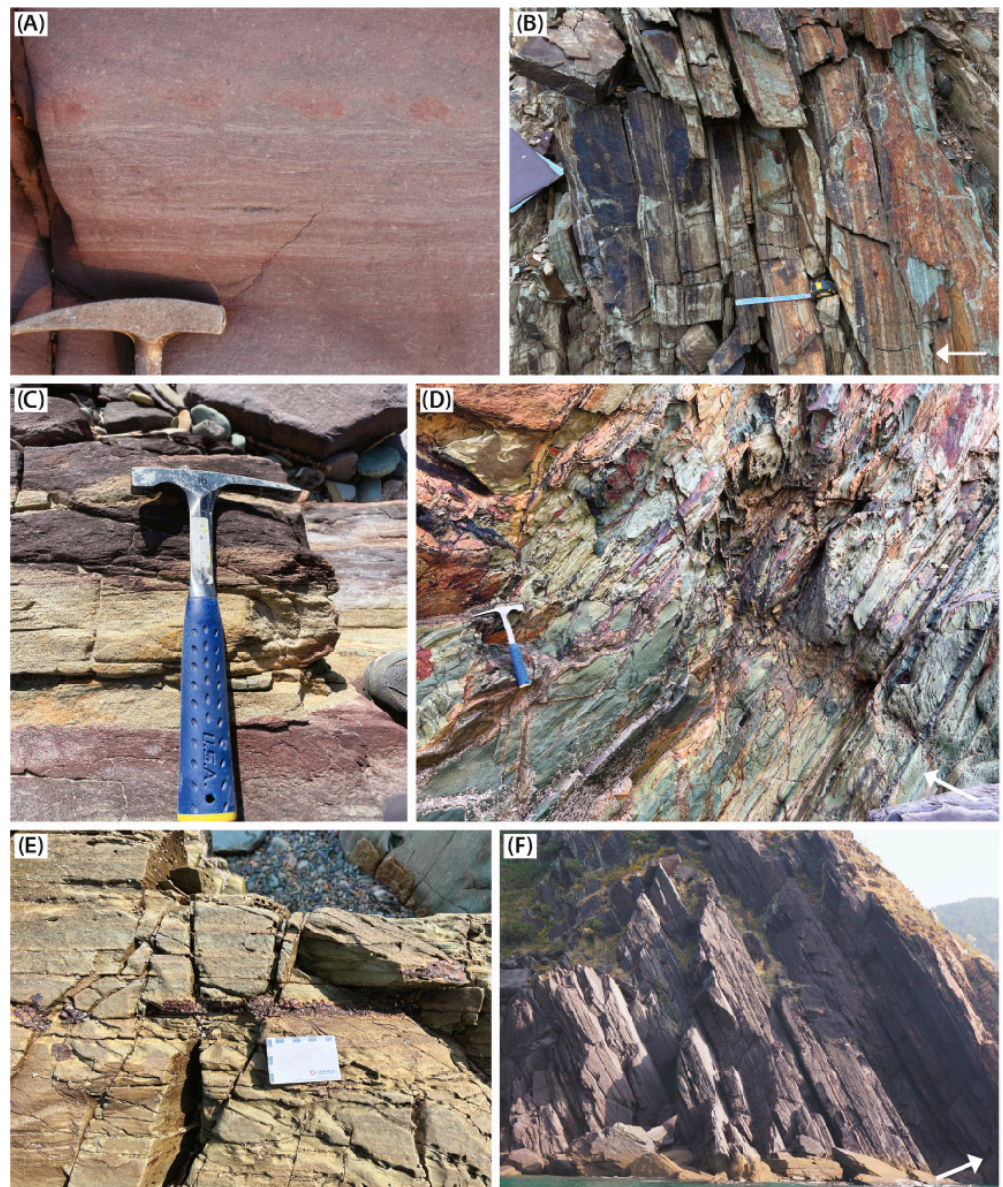


Figure 7. Photographs of the outcrops of redbeds and associated lithologies of Yedong Member, Socheong Formation. (A,B) Siltstone–mudstone couplets in (A) purple and (B) greenish-gray shales;

(C) siltstone–shale bed exhibiting gradual upward color change, from greenish-gray to purple, separated from the underlying purple shale by a sharp boundary; (D) hydrothermal veins in greenish-gray silty shale; (E) iron concretions in greenish-gray mudstone; (F) thickly developed purple shale beds below the upper boundary of Yedong Member.

4. Analytical Methods

4.1. Samples

Twelve rock samples were obtained from both the upper and lower units of the Yedong Member, Socheong Formation (Figure 1C, Table 1). Within the lower unit, four samples were collected, encompassing various lithologies such as sandstone, mudstone, silty shale, and others. In the upper unit, distinct color variations, including purple, red, greenish-gray, and dark gray, were observed in the beds, showcasing more pronounced differences compared with those in the lower unit of the Yedong Member. Consequently, the sampling process aimed to investigate the geochemical and mineralogical variances associated with these color differences. Notably, certain beds in the upper unit, particularly those exhibiting a greenish-gray color, contain metallic concretions. To thoroughly assess these features, a separate sample was taken from the beds with metallic concretions for further analysis (23SCD-03B).

Table 1. Major element compositions of the 12 samples analyzed in this study.

Analyte Symbol	SiO ₂	Al ₂ O ₃	Fe ₂ O _{3(T)}	MnO	MgO	CaO	Na ₂ O	K ₂ O	TiO ₂	P ₂ O ₅	LOI	Total	Lithology
Unit Symbol	%	%	%	%	%	%	%	%	%	%	%	%	
Detection Limit	0.01	0.01	0.01	0.005	0.01	0.01	0.01	0.01	0.001	0.01		0.01	
Analysis Method	FUS-ICP	FUS-ICP	FUS-ICP	FUS-ICP	FUS-ICP	FUS-ICP	FUS-ICP	FUS-ICP	FUS-ICP	FUS-ICP	GRAV	FUS-ICP	
Lower Unit													
23SCD-05	80.06	8.04	3.84	0.022	0.89	0.54	1.18	1.44	0.497	0.09	1.69	98.28	Sandstone
Sch-12	70.93	13.53	6.36	0.027	1.64	0.2	1.06	2.94	0.675	0.06	2.71	100.1	Mudstone
Sch-17A	65.3	17.64	4.81	0.024	1.64	0.05	0.84	4.86	1.217	0.04	3.55	99.97	Silty shale
SOD-19	74.2	9.09	4.95	0.082	1.48	2.89	0.91	1.86	0.459	0.04	4.12	100.1	Sandstone
Upper Unit													
23SCD-03A	50.32	20.68	16.19	0.114	1.78	0.29	0.44	3.63	2.121	0.21	4.12	99.9	Dark greenish-gray silty shale Part of 23SCD-
23SCD-03B	36.76	16.98	29.36	0.361	4.45	0.36	0.25	0.58	2.214	0.21	9.3	100.8	03A with metallic concretions
23SCD-03C	48.95	22.37	15.75	0.042	0.88	0.36	0.62	4.52	2.23	0.29	3.73	99.75	Purple shale
SOD-33	57.2	18.36	12.92	0.072	2.05	0.2	0.27	2.86	1.542	0.13	4.07	99.67	Purple shale
SOD-26	39.8	18.41	27.58	0.067	1.37	0.37	1.39	2.49	3.646	0.22	3.25	98.6	Purple shale
SOD-6	51.09	22.04	15.48	0.139	0.97	1.54	0.16	0.76	3.609	1.23	3.18	100.2	Greenish-gray silty shale
23SCD-04A	47.63	25.37	11.66	0.17	0.32	0.05	0.79	1.54	5.069	0.1	5.7	98.39	Greenish-gray silty shale
23SCD-04B	51.86	22.49	16.83	0.133	1.1	0.19	0.14	0.67	3.01	0.23	3.25	99.89	Greenish-gray silty shale

4.2. Bulk-Rock Geochemistry

We analyzed the bulk-rock geochemistry for 12 rock samples obtained from the Socheong Formation (Figure 1C). The analyses were performed at Activation Laboratories Ltd., in Ontario (Canada), using the 4LITHO (11+) QOP WRA/QOP WRA 4B2 package. The rock powders were fused with lithium metaborate/tetraborate, diluted with nitric acid, and analyzed using inductively coupled plasma optical emission spectroscopy (ICP-OES) and inductively coupled plasma mass spectrometry (ICP-MS). The accuracy of the results was evaluated by repeated analyses of the standard materials NIST 694, GBW07113, NOD-A-1, NOD-P-1, SY-4, BIR-1a, ZW-C, OREAS 101b, NCS DC86318, USZ 25-2006, DNC-1a, BCR-2, USZ 42-2006, REE-1, and W-2b (Supplementary Table S1). Ad-

ditional information about the procedure, precision, and accuracy of the analyses can be found at www.actlabs.com.

4.3. Mineralogy

The mineralogy of the representative lithologies was analyzed using a PANalytical X'pert Pro X-ray diffractometer at the Korea Institute of Ocean Science and Technology, using Cu-K α radiation generated at 45 kV and 30 mA. The powdered samples of the rocks were scanned from 3° to 55°, with a step size of 0.02° and a measuring speed of 1°/min, at room temperature. Data reduction was performed using the PANalytical Highscore Plus software version 4.1 (Malvern PANalytical) for pattern processing.

5. Analytical Results

The analytical results for the bulk-rock geochemistry of the 12 samples are listed in Tables 1 and 2. There is a notable distinction in the geochemical composition between the samples from the lower and upper units. Two sandstones (23SCD-05 and SOD-19) and two mudstones (Sch-12 and Sch-17A) from the lower, non-redbed unit of Socheong Formation exhibited SiO₂ contents of 65.30–80.06 wt %, Al₂O₃ contents of 8.04–17.64 wt %, and Fe₂O_{3(T)} contents of 3.84–6.36 wt %, indicating their ordinary siliciclastic origin. The siltstone and mudstone samples from the redbeds (23SCD-03C, SOD-33, and SOD-26) and intercalated greenish-gray beds (23SCD-03A, 23SCD-03B, SOD-6, 23SCD-04A, and 23SCD-04B) exhibited SiO₂ contents of 36.76–51.86 wt %, Al₂O₃ contents of 16.98–25.37 wt %, and Fe₂O_{3(T)} contents of 11.7–29.36 wt %. Figure 8 portrays the major elemental composition normalized to that of the upper continental crust. The rare earth element and yttrium (REY) compositions of the samples were normalized with respect to the post-Archean Australian Shale (PAAS; Taylor and McLennan, 1985) (Figure 9); Y was inserted between Dy and Ho according to its ionic radius [27].

Table 2. Rare earth element and yttrium contents of the 12 samples analyzed in this study.

Analyte Symbol	La	Ce	Pr	Nd	Sm	Eu	Gd	Tb	Dy	Ho	Er	Tm	Yb	Lu	Y
Unit Symbol	ppm														
Detection Limit	0.1	0.1	0.05	0.1	0.1	0.05	0.1	0.1	0.1	0.1	0.1	0.05	0.1	0.01	1
Analysis Method	FUS-MS	FUS-ICP													
Lower Unit															
23SCD-05	25.3	52	5.84	21.8	4.5	0.75	4.2	0.6	3.8	0.8	2.2	0.32	2	0.31	22
Sch-12	36.2	73.1	8.54	31.9	6.4	1.13	5.5	0.9	5.7	1.1	3.2	0.47	3.2	0.51	32
Sch-17A	46.6	91.4	10.4	39.2	7.5	1.36	6.1	1.1	6.8	1.4	4.2	0.64	4.3	0.7	41
SOD-19	24	49.3	5.78	22	4.5	0.79	3.9	0.6	3.9	0.8	2.2	0.31	2.1	0.34	22
Upper Unit															
23SCD-03A	31	47.7	8.31	30.9	6.5	1.87	5.9	1	6.5	1.3	3.5	0.5	3.2	0.48	32
23SCD-03B	96.2	371	21.4	81.5	16.4	4.49	14.3	1.8	9.1	1.5	4	0.53	3.3	0.51	38
23SCD-03C	120	251	28.9	109	19.5	4.63	14.7	1.9	10.6	2	5.6	0.79	5.2	0.79	53
SOD-33	46.8	93.9	10.8	39.9	7.5	1.21	5.9	1	6.7	1.4	4.4	0.67	4.4	0.7	36
SOD-26	24.7	53.4	6.1	24.8	5.5	2.18	6.1	1.1	7.3	1.4	3.9	0.54	3.4	0.56	33
SOD-6	63.3	130	15	59.7	12	4.02	11	1.7	9.6	1.7	4.7	0.65	4	0.63	49
23SCD-04A	70.6	153	18.2	72.8	13.8	3.54	10.4	1.4	8.1	1.6	4.5	0.63	4.2	0.66	44
23SCD-04B	77.9	176	21	84.9	15.2	3.71	11.2	1.5	9.1	1.8	4.8	0.67	4.5	0.66	47

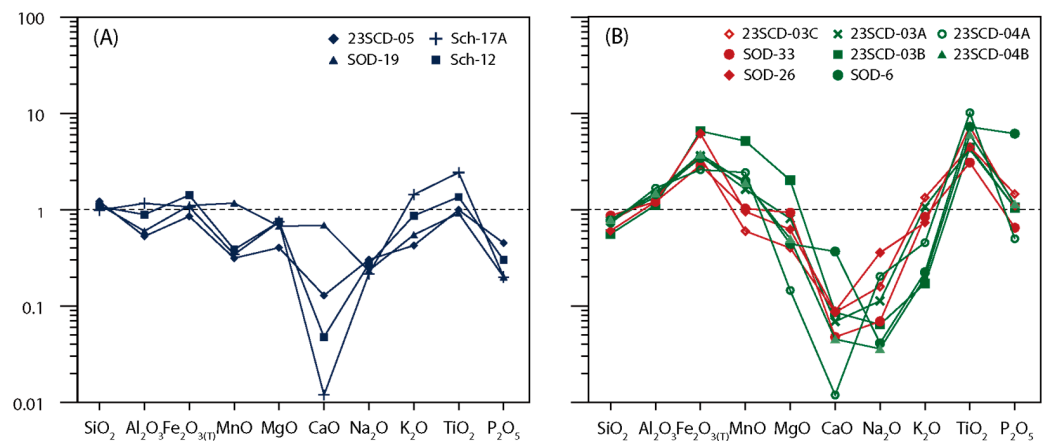


Figure 8. Major elemental compositions of the samples normalized to that of the upper continental crust of Socheong Formation (**A**: lower unit; **B**: upper unit). The symbols in panel B are color-coded to correspond with the bed colors; e.g., red represents red or purple beds, and green represents greenish-gray or dark greenish-gray beds.

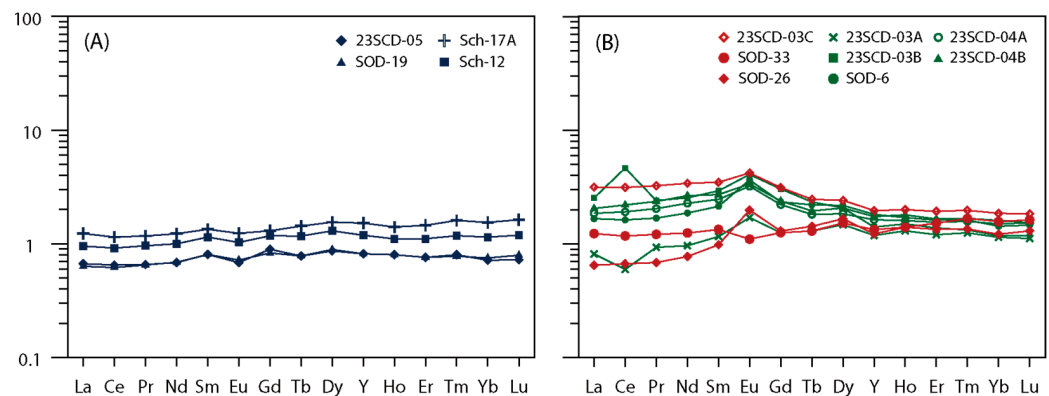


Figure 9. Rare earth element (REE) composition normalized to the post-Archean Australian Shale for (A) lower unit and (B) upper unit of Yedong Member, Socheong Formation.

X-ray diffraction (XRD) patterns and petrographic thin-section photos of the Socheong Formation are shown in Figures 10 and 11, respectively. The dark gray mudstone (Sch-12) from the lower unit exhibited characteristic quartz peaks, with the small peaks being hardly identifiable (Figure 10A). The thin section of the dark greenish-gray silty shale sample (23SCD-03A) from the upper unit is shown in Figure 11A; with respect to the XRD analysis, the sample exhibited peaks at ~ 14.1 , ~ 7.1 , ~ 4.7 and ~ 3.56 Å, which could be attributed to the (001), (002), (003), and (004) basal reflections of chlorite (Figure 10B). The relative intensities of the (001) and (003) reflections were considerably lower than those of the (002) and (004) reflections, indicating that chamosite, an Fe-rich end-member of chlorite, was the dominant component of the sample. The purple shale sample (SOD-26) of the upper unit exhibited the characteristic peaks of hematite (Figure 10C), indicated in the thin section by a dark color (Figure 11B), in addition to the characteristic peaks of quartz and muscovite/illite (Figure 10C). The greenish-gray siltstone samples (23SCD-04A and 23SCD-04B) of the upper unit exhibited characteristic peaks of chloritoid at ~ 4.45 Å ($\sim 20^\circ 2\theta$), pyrophyllite at ~ 9.2 , ~ 4.6 , and ~ 3.1 Å ($\sim 9.6^\circ$, 19.3° and $29.1^\circ 2\theta$), and chlorite (Figure 10D,E); these minerals were observed in the petrographic thin-section analysis as well (Figure 11C,D).

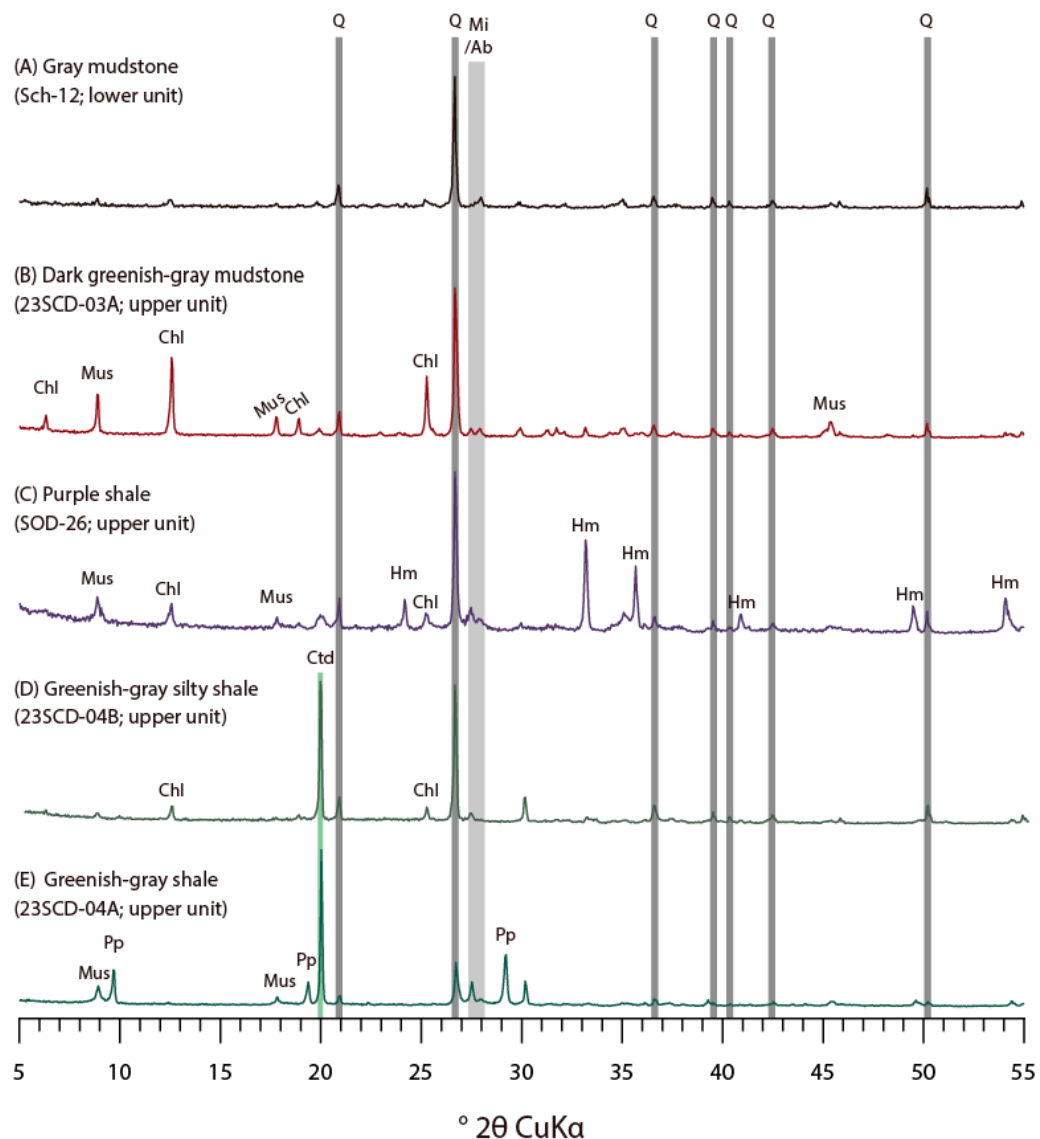


Figure 10. X-ray diffraction (XRD) results of the representative samples of Socheong Formation: (A) Gray mudstone sample (Sch-12) of lower unit; (B–E) representative samples of Fe-rich upper unit for (B) 23SCD-03A, (C) SOD-26, (D) 23SCD-04B, and (E) 23SCD-04A. Q = quartz, Mi/Ab = microcline/albite, Chl = chlorite, Mus = muscovite and illite, Hm = hematite, Ctd = chloritoid, and Pp = pyrophyllite.

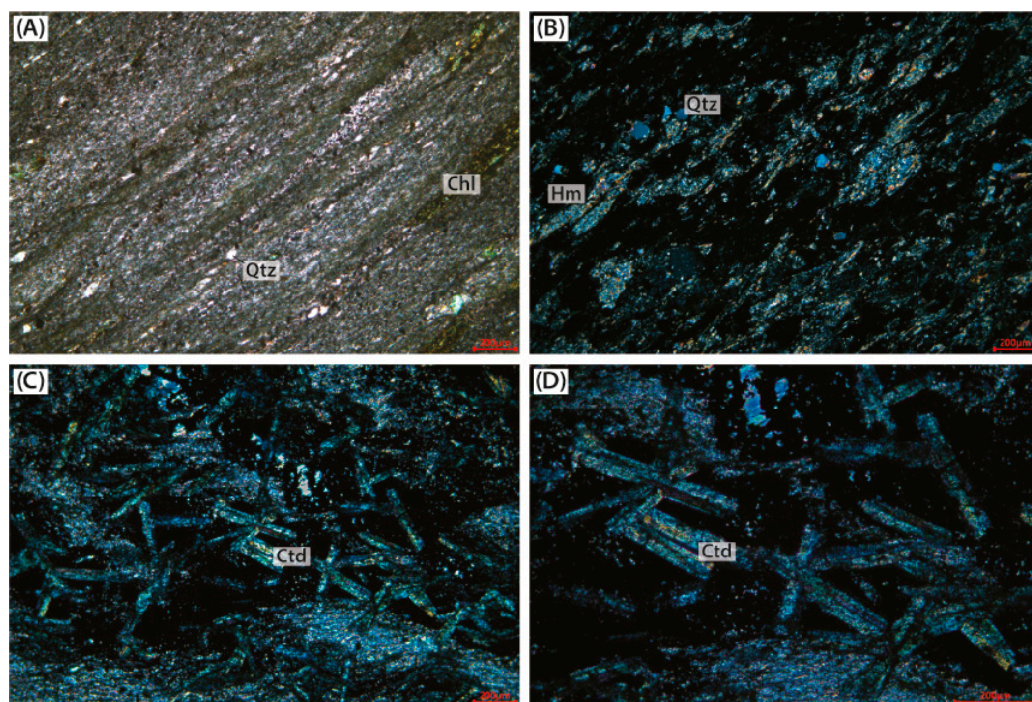


Figure 11. Photographs of thin sections of Fe-enriched upper unit samples: (A) dark greenish-gray silty shale (23SCD-03A, PPL); (B) purple shale (SOD-26); and (C,D) greenish-gray silty shale (23SCD-04A), after magnification. Q = quartz, Chl = chlorite, Hm = hematite and Ctd = chloritoid.

6. Discussion

6.1. Hydrothermal Input of Fe

The redbeds and co-occurring greenish-gray siltstone–mudstones of the upper unit contained 18.2% $\text{Fe}_2\text{O}_{3(\text{T})}$ on average (with 12.7% Fe) (Table 1), which is significantly enriched compared with those of UCC (Figure 8). The purple shale sample (SOD-33) contained 29.4% of $\text{Fe}_2\text{O}_{3(\text{T})}$ (19.29% Fe); thus, the rock can be termed “ironstone,” based on the definition proposed in previous studies [28,29]. The high $\text{Fe}_2\text{O}_{3(\text{T})}$ contents (Table 1, Figure 8B) and Fe/Al ratios (Figure 12A) for the samples obtained from the upper unit suggest an additional input of Fe, other than from the detrital source. The positive Eu anomalies [$\text{Eu}/\text{Eu}^*_{\text{SN}} = (\text{Eu}_{\text{SN}} / (0.67\text{Sm}_{\text{SN}} + 0.33\text{Tb}_{\text{SN}}))$] for most samples of the Fe-rich upper unit indicated a hydrothermal source of Fe (Figure 12B), supported by the general covariance of the Eu anomaly and $\text{Fe}_2\text{O}_{3(\text{T})}$. In contrast, the Fe content of the lower unit of the Yedong Member is similar to that of the upper continental crust (Figure 8A). The small negative Eu anomalies and Fe/Al ratios, similar to those observed for the PAAS, indicate a negligible influence of the hydrothermal fluid.

A conceivable detrital source of Fe is the mafic sills reported in the Baengnyeong and Daecheong islands; in particular, the source can be the Baengnyeong Sill strata [10], because the intrusion age of the Baengnyeong Sill (ca. 940 Ma) is largely concurrent with the maximum ages of the detrital zircons found in the Socheong Formation (ca. 930–880 Ma; Figure 2B,C). However, the total Fe content, represented as $\text{Fe}_2\text{O}_{3(\text{T})}$, of the Baengnyeong Sill sample was 13.8–16.9 wt % [10], generally lower than those of the Fe-rich units of Socheong Formation. The Eu anomaly was not apparent in the Baengnyeong Sill [10], either, negating its possibility as a direct detrital source for the Fe-rich upper unit of the Socheong Formation.

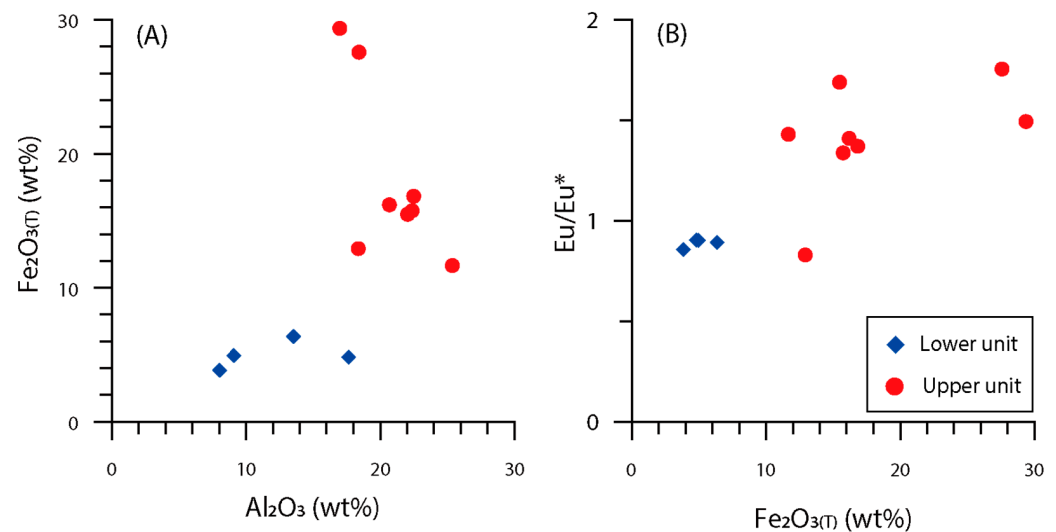


Figure 12. Cross-plots of (A) $\text{Fe}_2\text{O}_{3(\text{T})}$ versus Al_2O_3 and (B) Eu/Eu^* versus Fe_2O_3 of upper and lower units of Yedong Member, Socheong Formation.

In the greenish-gray shale samples (SOD-6, 23SCD-04A and 23SCD-04B) of the upper unit, chloritoid porphyroblasts were detected in the XRD patterns and observed in the petrographic thin sections as well (Figure 10D,E and Figure 11C,D, respectively). Chloritoid, a neosilicate mineral represented by the general formula $(\text{Fe},\text{Mg},\text{Mn})_2\text{Al}_4\text{Si}_2\text{O}_{10}(\text{OH})_4$, is generally found in metamorphic rocks of various grades ranging from sub-greenschist to amphibolite facies [30]. The Socheong Formation is considered to have undergone sub-greenschist facies metamorphism, indicated by the absence of textural schistosity or high-grade metamorphic minerals. The chloritoids in the Socheong Formation can be associated with chamosite and white mica (presumably pyrophyllite or muscovite) (Figure 10), indicating low-grade metamorphism. Although chloritoids are more commonly associated with higher-grade metamorphic index minerals, such as andalusite, kyanite, and staurolite [31], hydrothermal activity has been reported to induce the growth of chloritoid minerals [32]. The low-grade metamorphic ensemble of chloritoid, chlorite, and muscovite of the upper unit of the Yedong Member, Socheong Formation indicates Fe enrichment and high contents of Al [30,33–35], which can be explained by the addition of hydrothermal iron to Al-rich pelitic rocks.

6.2. Bottom Redox Conditions

The differential redox sensitivities and ionic radii of REY compositions result in the relative enrichment and/or depletion of light rare earth elements (LREEs), Ce, and Y in the bulk sediment. The negative Ce anomaly, $[\text{Ce}/\text{Ce}^*_{\text{SN}} = \text{Ce}_{\text{SN}} / (0.5\text{La}_{\text{SN}} + 0.5\text{Pr}_{\text{SN}})]$, and the depletion of LREEs over heavy rare earth elements (HREEs) is typical for modern oxidized ocean water, because of the preferential incorporation of Ce^{4+} and the scavenging of LREEs by rapidly oxidized Fe–Mn oxyhydroxides [36,37]. The behavior of Y was somewhat inverse to those of the LREEs and Ce. Notably, Ho, the geochemical analog of Y, is more reactive than Y; thus, Y is enriched in seawater when normalized to the average shale composition [38]. In the redox-stratified ocean, a negative Ce anomaly and positive Y anomaly and LREE depletion are expected to occur above the redoxcline, where the oxidizing environment prevails; the opposite is expected to occur below the redoxcline [37]. Significant variabilities in LREE depletion and Ce and Y anomalies are apparent in Fe-rich beds, suggesting that the beds have been deposited near the redoxcline, where the adsorption–remobilization reactions are the most active. Such characteristics in the REY are similar to those of hydrothermally influenced sediments near the redox boundary deposited after the Late Paleoproterozoic [37]. In contrast, flat REY patterns and a lack of

Ce and Y anomalies were observed for the samples of the lower unit of the Yedong Member (Figure 10A).

The repetitive occurrence of greenish-gray and purple strata (Figure 7) in the upper unit of the Yedong Member also indicates episodic hydrothermal activity and the consequent variation in the redox state of the basin. During the deposition of the upper unit, an overall oxygenated bottom water condition is inferred, as evidenced by the presence of thickly developed red or purple shale overlain by the substantial limestone unit (i.e., Bunbawi Member). Episodic hydrothermal fluids may have contributed to brief periods of anoxia that dissipated rapidly. There is a gradual change in color from the greenish-gray bottom to the purple top of the bed (Figure 7C), sharply underlain by another greenish-gray colored bed. This can be explained by intermittent hydrothermal activity, which not only supplied Fe^{2+} , but also generated short-lived anoxia in the basin, resulting in a greenish-gray or dark gray mudstone layer. The green color of the rock can be attributed to the presence of ferrous clay minerals (chamositic chlorite). After the anoxia dissipated, Fe^{2+} was oxidized at the water–sediment interface; the red-purple color of the mudstones could be attributed to the presence of hematite (Figure 10C). The alteration of purple and greenish-dark gray mudstone beds disappeared upward, and the purple shale developed thickly in the uppermost strata of the Yedong Member (Figure 7F). Notably, in the uppermost strata of the Yedong Member of the Socheong Formation, purple shale diminishes progressively, alternating with stromatolite-bearing limestone beds (Figure 6A) and eventually transforming into thick limestone (Bunbawi Member). This indicates that the hydrothermally driven anoxia ceased to exist, because the deposition of redbed and stromatolite-bearing limestone occurred in photic, oxygenated, yet Fe-enriched surface water. One may suggest that the colors of the beds only reflect the water depths of deposition; however, this possibility is negated by their similarity in sedimentary structures and the development of mudcracks (Figure 5D,E), in both the greenish-gray and purple shales. Thus, the color transition in the shale unit can only be explained by Fe addition, and the relevant bottom redox condition changes can be attributed to intermittent hydrothermal activity.

6.3. Genetic Linkage of Fe-Rich Beds and the Dashigou Large Igneous Provinces (LIP)

Because Fe is easily precipitated in an oxic environment, the excess Fe supplied by hydrothermal activity in the modern, nearly fully oxidized open ocean basin would be accumulated near the vents in the form of oxyhydroxides. However, under anoxic conditions (e.g., below the redoxcline), excessive Fe can be mobilized as Fe^{2+} or only partly deposited in the sulfide phases. Such mobilization of Fe would result in the enrichment of dissolved Fe in the basin, which would eventually lead to the deposition of iron-rich formations or ironstones, if sufficiently oxidized. In Archean and Early Paleoproterozoic oceans, wherein anoxia prevailed, iron oxygenation was largely mediated by microbes or photochemical reactions in reducing conditions, resulting in the deposition of banded iron formations [20,37,39]. In the Late Neoproterozoic and modern Phanerozoic ocean, after the rise of atmospheric oxygen during the Neoproterozoic Oxygenation Event (~850–540 Ma), a sufficient amount of Fe^{2+} delivery was achieved in small semi-isolated basins, favoring the formation of ironstones [20,39]. Consequently, their formation can be likely linked to anoxic events in several cases, as exemplified by the Snowball Earth events [40]. During the Mesoproterozoic–Early Neoproterozoic (~1.85–0.75 Ga), the ocean redox condition is assumed to be between these two extremes, which was less reducing than the Archean and the Early Paleoproterozoic but notably more reducing than the Phanerozoic Ocean [20,37,39]. Even after the Great Oxygenation Event, at 2.32 Ga [39], deep-ocean anoxic conditions might have been preserved in isolated–semi-isolated basins, even if the surface ocean was oxygenated [20]. Notably, differential oxygenation generates a redox stratification and developed a “redoxcline” in the water column, which is favorable for the formation of Fe-rich beds in the presence of large hydrothermal fluxes of Fe [20,37,39].

The delivery of an excessive amount of Fe^{2+} into these semi-isolated redox-stratified basins may have been achieved through mafic igneous activities. Iron-rich formations

and ironstones are often genetically linked to an excessive Fe supply from volcanic and hydrothermal activities [20,39,41,42]. The deposition of large and economically important iron formations commonly coincides with mantle-plume breakout events, as recorded by the occurrence of LIPs, dike swarms, and submarine mafic volcanic rocks [20,41]. In the study area, relevant mafic igneous activity was recorded at ~890 Ma in a doleritic sill on Socheong Island, corresponding to the Sariwon Sill of the Pyeongnam Basin [10,12]. Its intrusion age is vaguely discernible from the maximum depositional age of the Socheong Formation (~900 Ma), based on the youngest detrital zircon ages of the upper unit of the Yedong Member (SOD-6, Figure 2C), with respect to the precision of $^{207}\text{Pb}/^{206}\text{Pb}$ ages [10]. The age distribution of the SOD-6 sample was characterized by a predominant 930–880 Ma peak, devoid of any other age peaks identified in the lower unit of the Yedong Member (SOD-19, Figure 2B), exhibiting similar age distribution patterns to those of the Baengnyeong and Daecheong groups [19]. This difference indicates a significant change in the provenance of the detritus during the deposition of the Yedong Member, involving syn- or near-depositional extrusive magmatism that could have supplied the zircons (of age 900 Ma). Although no mafic extrusive rocks have been found on Socheong Island, it is likely that magmatic events accompanying hydrothermal activity occurred during the deposition of the Socheong Formation before the sill intrusion.

In the southern Pyeongnam Basin of mainland North Korea, reddish-purple sericite-chlorite phyllite has been reported in the upper Seolhwasan (Solhwasan) Formation, which is underlain by the limestone-dominated Okhyeonri (Okhyonri) Formation of the Mukcheon (Mukchon) Group [22]. The similarity in the lithologic associations between the Yedong and Bunbawi members of the Socheong Formation and the Seolhwasan and Okhyeonri formations is consistent with the existing hypothesis of their stratigraphic affinity [23]. The deposition of Fe-rich beds was presumably widespread, at least in the southern Pyeongnam Basin, during the deposition of the Socheong and Okhyeonri formations, which can be attributed to mafic igneous activities in the region.

6.4. Regional Concurrency of the Formation of the Redbeds and Dashigou Large Igneous Province (LIP) and the Stratigraphic Implications

The mafic sill intrusions in the Pyeongnam Basin are thought to have originated from the mantle plume involved in the formation of the Dashigou LIP, as evidenced by the widespread intrusions of mafic dikes and swarms in the Xu-Huai, Dalian, and Pyeongnam basins [1,4,7,10,12]. Although there should have been some degree of inter-basinal differences with respect to the timings of mafic igneous activities, the intensity of hydrothermal activity and sensitivity to the changes in redox states, as evidence of Fe enrichment in sedimentary strata, was noted in various regions of the eastern SKC. For instance, red or purple shales have been reported in the Shisanlitai Formation of the Jinxian Group in the Dalian Basin [17,43] and the Shijia Formation of the Huaibei Group in the Xu-Huai Basin [16]. The occurrence of red limestones in the eastern and southern SKC during the Tonian Period was also reported by Kuang et al. [44], supporting the theory of the occurrence of basin-wide hydrothermal Fe-enrichment.

Given the paucity of precise age-determination methods for Proterozoic strata, the extensive occurrence of redbeds indicates their potential as marker beds for regional stratigraphic correlation. However, previous studies recognize at least three different magmatic activities involved in the Dashigou LIP, at 940, 920, and 890 Ma [10], in the Pyeongnam, Dalian, and Xu-Huai basins, respectively, corroborating that the repetitive occurrences of redbeds may be due to magmatic Fe supply. For instance, the Obongri Formation of the Jikhyeon Group, which has a correlation with the Baengnyeong and Daecheong groups, contains reddish-purple shale or phyllite [22]. The timing of this redbed deposition was estimated to be 1000–940 Ma, preceding the formation of the Socheong Formation by at least 60 million years [10]. Although the field investigation searching for the further presence of the redbeds in the individual basins is beyond the aims of this study, and thus not attempted in this work, their synchronicity can be supplemented by carrying out $\delta^{13}\text{C}$ chemostratigra-

phy analysis. Interestingly, the Majiatun anomaly at approximately 950–920 Ma, suggested to be the oldest known Neoproterozoic nCIE event in eastern SKC [17], can be identified within the red stromatolite-bearing dolostone and limestone associated with the abovementioned red shale beds [44]. Likewise, a nCIE has been documented in the Seolhwasan and Okhyeonri formations of Mukcheon Group in southern Pyeongnam Basin, presumably correlated to the Socheong Formation. This occurrence aligns with the presence of red-purple shale and limestone layers [15]. Therefore, the correspondence of $\delta^{13}\text{C}$ negative excursion event in the redbeds can be a stratigraphically diagnostic feature. The genetic relationship between redbed occurrence and $\delta^{13}\text{C}$ negative excursion events can be an interesting topic for future studies in marine biology, paleontology, and/or related fields, as Fe addition and bottom anoxia induced by hydrothermal activities may have a significant influence on the microbial community.

7. Conclusions

Our study is the first to report the occurrence of redbeds in the Early Neoproterozoic Socheong Formation. The geochemical and mineralogical characteristics of the redbeds indicated that the source of Fe was hydrothermal fluids from mafic igneous activities. Hydrothermal inputs generated episodic temporal anoxia in the redox-stratified semi-isolated basins in the study area, even though the surface waters of the basins were oxygenated, resulting in the intercalation of chamositic and hematitic ferruginous ironstone beds. The Fe-enriched hydrothermal fluids likely originated from the mafic igneous activities involved in the emplacement of the Dashigou LIP in the Sangwon Supergroup. With a strong correlation with nCIE events, the occurrence of redbeds has been reported in various strata of the Sangwon, Xu-Huai, and Dalian basins; thus, the redbeds can be used as a diagnostic feature for stratigraphic correlation. The occurrence of hydrothermally driven anoxia and Fe addition further supports the existing hypotheses that the formation of the Dashigou LIP had a great influence on the biosphere and seawater chemistry in the region, even during the Proterozoic period.

Supplementary Materials: The following supporting information can be downloaded at: <https://www.mdpi.com/article/10.3390/min14010059/s1>, Table S1. Quality control details of geochemical analyses.

Author Contributions: Conceptualization, H.Y. and I.S.; investigation, H.Y. and S.H.L.; formal analysis, H.Y. and S.H.L.; writing—original draft preparation, H.Y.; writing—review and editing, I.S.; visualization, H.Y.; supervision, I.S.; funding acquisition, I.S. and S.H.L. All authors have read and agreed to the published version of the manuscript.

Funding: This study was supported by the Marine Environment Division of the Incheon Metropolitan City, Republic of Korea and the Basic Research Project of KIGAM (GP2020-003) funded by the Ministry of Science and ICT, Republic of Korea.

Data Availability Statement: Data are contained within the article.

Acknowledgments: The authors would like to thank Jae Yong Jeong, Jun Hyuk Seo, and Euijong Lee for their assistance in fieldwork and experimental setup, and Jeong-Hyun Lee, Hyojong Lee, and Deung-Lyong Cho for their informative discussions and photo courtesy.

Conflicts of Interest: The authors declare no conflicts of interest.

References

1. Peng, P. Late Paleoproterozoic–Neoproterozoic (1800–541 Ma) Mafic Dyke Swarms and Rifts in North China. In *Precambrian Geology of China*; Zhai, M., Ed.; Springer: Berlin/Heidelberg, Germany, 2015; pp. 171–204.
2. Hu, B.; Zhai, M.; Li, T.; Li, Z.; Peng, P.; Guo, J.; Kusky, T.M. Mesoproterozoic magmatic events in the eastern North China Craton and their tectonic implications: Geochronological evidence from detrital zircons in the Shandong Peninsula and North Korea. *Gondwana Res.* **2012**, *22*, 828–842. [[CrossRef](#)]
3. Hu, J.; Li, Z.; Gong, W.; Hu, G.; Dong, X. Meso–Neoproterozoic Stratigraphic and Tectonic Framework of the North China Craton. In *Main Tectonic Events and Metallogeny of the North China Craton*; Zhai, M., Zhao, Y., Zhao, T., Eds.; Springer: Singapore, 2016; pp. 393–422.

4. Peng, P. Precambrian mafic dyke swarms in the North China Craton and their geological implications. *Sci. China Earth Sci.* **2015**, *58*, 649–675. [[CrossRef](#)]
5. Peng, P.; Zhai, M.-G.; Li, Q.; Wu, F.; Hou, Q.; Li, Z.; Li, T.; Zhang, Y. Neoproterozoic (~900 Ma) Sariwon sills in North Korea: Geochronology, geochemistry and implications for the evolution of the south-eastern margin of the North China Craton. *Gondwana Res.* **2011**, *20*, 243–254. [[CrossRef](#)]
6. Peng, P.; Hu, B.; Zhang, Z.Y.; Zhang, Y.B.; Guo, J.H.; Zhai, M.G. Review on geological evolution of the Pyongnam basin in Korean Peninsula. *Acta Petrol. Sin.* **2021**, *37*, 129–142. [[CrossRef](#)]
7. Su, X.; Peng, P.; Foley, S.; Teixeira, W.; Zhai, M.-G. Initiation of continental breakup documented in evolution of the magma plumbing system of the ca. 925 Ma Dashigou large igneous province, North China. *Lithos* **2021**, *384–385*, 105984. [[CrossRef](#)]
8. Sun, F.; Peng, P.; Zheng, D.; Zuo, P. Reappraising the Provenance of Early Neoproterozoic Strata in the Southern–Southeastern North China Craton and Its Implication for Paleogeographic Reconstruction. *Minerals* **2022**, *12*, 510. [[CrossRef](#)]
9. Zhai, M.; Zhang, X.-H.; Zhang, Y.-B.; Wu, F.-Y.; Peng, P.; Li, Q.-L.; Li, Z.; Guo, J.; Li, T.-S.; Zhao, L.; et al. The geology of North Korea: An overview. *Earth Sci. Rev.* **2019**, *194*, 57–96. [[CrossRef](#)]
10. Cho, D.-L.; Peng, P.; Hwan Lee, S.; Park, J.-Y.; Seo, I.; Sun, F.; Li, Q.; Zhang, Y. Identify vestiges of large igneous provinces in deep time: A 0.9 Ga case from North China (Sino-Korean) craton. *Precambrian Res.* **2023**, *398*, 107220. [[CrossRef](#)]
11. Ernst, R.E. *Large Igneous Provinces*; Cambridge University Press: Cambridge, UK, 2014.
12. Peng, P.; Bleeker, W.; Ernst, R.E.; Söderlund, U.; McNicoll, V. U–Pb baddeleyite ages, distribution and geochemistry of 925Ma mafic dykes and 900Ma sills in the North China craton: Evidence for a Neoproterozoic mantle plume. *Lithos* **2011**, *127*, 210–221. [[CrossRef](#)]
13. Zhao, H.; Zhang, S.; Ding, J.; Chang, L.; Ren, Q.; Li, H.; Yang, T.; Wu, H. New geochronologic and paleomagnetic results from early Neoproterozoic mafic sills and late Mesoproterozoic to early Neoproterozoic successions in the eastern North China Craton, and implications for the reconstruction of Rodinia. *GSA Bull.* **2020**, *132*, 739–766. [[CrossRef](#)]
14. Ernst, R.E.; Youbi, N. How Large Igneous Provinces affect global climate, sometimes cause mass extinctions, and represent natural markers in the geological record. *Palaeogeogr. Palaeoclimatol. Palaeoecol.* **2017**, *478*, 30–52. [[CrossRef](#)]
15. Park, H.U.; Zhai, M.G.; Yang, J.H.; Peng, P.; Kim, J.N.; Zhang, Y.B.; Kim, M.C.; Park, U.; Feng, L.J. Deposition age of the Sangwon supergroup in the Pyongnam Basin (Korea) and the Early Tonian negative carbon isotope interval. *Acta Petrol. Sin.* **2016**, *32*, 2181–2195.
16. Xiao, S.; Shen, B.; Tang, Q.; Kaufman, A.J.; Yuan, X.; Li, J.; Qian, M. Biostratigraphic and chemostratigraphic constraints on the age of early Neoproterozoic carbonate successions in North China. *Precambrian Res.* **2014**, *246*, 208–225. [[CrossRef](#)]
17. Zhang, Z.; Peng, P.; Feng, L.; Gong, Z.; Mitchell, R.N.; Li, Y. Oldest-known Neoproterozoic carbon isotope excursion: Earlier onset of Neoproterozoic carbon cycle volatility. *Gondwana Res.* **2021**, *94*, 1–11. [[CrossRef](#)]
18. Kim, S.W.; Kwon, S.; Santosh, M.; Cho, D.-L.; Kee, W.-S.; Lee, S.-B.; Jeong, Y.-J. Detrital zircon U-Pb and Hf isotope characteristics of the Early Neoproterozoic successions in the central-western Korean Peninsula: Implication for the Precambrian tectonic history of East Asia. *Precambrian Res.* **2019**, *322*, 24–41. [[CrossRef](#)]
19. Cho, D.-L.; Lee, S.H.; Park, J.-Y. *Geological Report of the Baengnyeongdo·Daecheongdo·Socheongdo sheets (1:50,000)*; Korea Institute of Geoscience and Mineral Resources: Daejeon, Republic of Korea, 2021; p. 73.
20. Bekker, A.; Planavsky, N.J.; Krapež, B.; Rasmussen, B.; Hofmann, A.; Slack, J.F.; Rouxel, O.J.; Konhäuser, K.O. 9.18—Iron Formations: Their Origins and Implications for Ancient Seawater Chemistry. In *Treatise on Geochemistry*, 2nd ed.; Holland, H.D., Turekian, K.K., Eds.; Elsevier: Oxford, UK, 2014; pp. 561–628.
21. Lim, S.-B.; Choi, H.-I.; Kim, B.C.; Kim, J.C. *Depositional systems of the sedimentary basins (I): Depositional systems and their evolution of the Proterozoic Paegryeong Group and Taean Formation*; KIGAM Annual Report; Korea Institute of Geoscience and Mineral Resources: Daejeon, Republic of Korea, 1999; p. 116.
22. Paek, R.J.; Kang, H.G.; Jon, G.P.; Kim, Y.M.; Kim, Y.H. *Geology of Korea*; Foreign Languages Books Publishing House: Pyongyang, Republic of Korea, 1993; p. 631.
23. Kim, J.-Y.; Kim, T.-S. Occurrence and Geological Significance of Stromatolites from the Precambrian Strata in the Socheong Island, Incheon, Korea. *J. Korean Earth Sci. Soc.* **1999**, *20*, 111–125.
24. Lee, S.J.; Kim, J.; Lee, K.C. Bacterial microfossils from Precambrian sedimentary rocks, Socheong Island, Korea. *J. Geol. Soc. Korea* **2003**, *39*, 171–182.
25. Kim, J.-Y.; Kim, K.-S.; Kim, T.-S. Raindrop imprints from the Late Proterozoic Sangwon System of the Socheong Island of Ongjin-gun, Incheon, Korea. *J. Korean Earth Sci. Soc.* **1999**, *20*, 55–60.
26. Kong, D.-Y.; Lee, S.-J. Possibility for Heliotropism from Inclined Columns of Stromatolites, Socheong Island, Korea. *J. Korean Earth Sci. Soc.* **2013**, *34*, 381–392. [[CrossRef](#)]
27. Bau, M.; Dulski, P. Distribution of yttrium and rare-earth elements in the Penge and Kuruman iron-formations, Transvaal Supergroup, South Africa. *Precambrian Res.* **1996**, *79*, 37–55. [[CrossRef](#)]
28. Gross, G.A. A classification of iron formations based on depositional environments. *Can. Mineral.* **1980**, *18*, 215–222.
29. James, H.L. Sedimentary facies of iron-formation. *Econ. Geol.* **1954**, *49*, 235–293. [[CrossRef](#)]
30. Castellanos-Alarcón, O.M.; Ríos-Reyes, C.A.; García-Ramírez, C.A. Occurrence of chloritoid-bearing metapelitic rocks and their significance in the metamorphism of the Silgará Formation at the Central Santander Massif. *Bol. Cienc. Tierra* **2016**, 5–15. [[CrossRef](#)]

31. Spear, F.S. *Metamorphic Phase Equilibria and Pressure-Temperature-Time Paths*/Frank S. Spear, 2nd ed.; Mineralogical Society of America: Washington, DC, USA, 1995; p. 799.
32. Ochoa, M.; Arribas, J.; Mas, R.; Goldstein, R.H. Destruction of a fluvial reservoir by hydrothermal activity (Camerós Basin, Spain). *Sediment. Geol.* **2007**, *202*, 158–173. [[CrossRef](#)]
33. Johnson, T.E.; Brown, M.; Solar, G.S. Low-pressure subsolidus and suprasolidus phase equilibria in the MnNCKFMASH system: Constraints on conditions of regional metamorphism in western Maine, northern Appalachians. *Am. Mineral.* **2003**, *88*, 624–638. [[CrossRef](#)]
34. Primmer, T.J. A transition from diagenesis to greenschist facies within a major Variscan fold/thrust complex in SW England. *Mineral. Mag.* **1985**, *49*, 365–374. [[CrossRef](#)]
35. Turner, F.J.; Verhoogen, J. *Igneous and Metamorphic Petrology*, 2nd ed.; McGraw-Hill: New York, NY, USA, 1960.
36. German, C.R.; Elderfield, H. Application of the Ce anomaly as a paleoredox indicator: The ground rules. *Paleoceanography* **1990**, *5*, 823–833. [[CrossRef](#)]
37. Planavsky, N.; Bekker, A.; Rouxel, O.J.; Kamber, B.; Hofmann, A.; Knudsen, A.; Lyons, T.W. Rare Earth Element and yttrium compositions of Archean and Paleoproterozoic Fe formations revisited: New perspectives on the significance and mechanisms of deposition. *Geochim. Cosmochim. Acta* **2010**, *74*, 6387–6405. [[CrossRef](#)]
38. Bau, M.; Möller, P.; Dulski, P. Yttrium and lanthanides in eastern Mediterranean seawater and their fractionation during redox-cycling. *Mar. Chem.* **1997**, *56*, 123–131. [[CrossRef](#)]
39. Bekker, A.; Slack, J.F.; Planavsky, N.; Krapez, B.; Hofmann, A.; Konhäuser, K.O.; Rouxel, O.J. Iron Formation: The Sedimentary Product of a Complex Interplay among Mantle, Tectonic, Oceanic, and Biospheric Processes*. *Econ. Geol.* **2010**, *105*, 467–508. [[CrossRef](#)]
40. Kump, L.R.; Seyfried, W.E. Hydrothermal Fe fluxes during the Precambrian: Effect of low oceanic sulfate concentrations and low hydrostatic pressure on the composition of black smokers. *Earth Planet. Sci. Lett.* **2005**, *235*, 654–662. [[CrossRef](#)]
41. Isley, A.E.; Abbott, D.H. Plume-related mafic volcanism and the deposition of banded iron formation. *J. Geophys. Res. Solid Earth* **1999**, *104*, 15461–15477. [[CrossRef](#)]
42. Klein, C.; Beukes, N.J.; Holland, H.D.; Kasting, J.F.; Kump, L.R.; Lowe, D.R. Proterozoic Atmosphere and Ocean. In *The Proterozoic Biosphere: A Multidisciplinary Study*; Klein, C., Schopf, J.W., Eds.; Cambridge University Press: Cambridge, UK, 1992; pp. 135–174.
43. Wu, Z.; Zhang, G.; Gao, F.; Wang, H.; Qiu, L.; Sun, Q.; Yu, F.; Zhong, M. Sequence stratigraphic division of the Shisanlitai Formation of Neoproterozoic in Southern Liaoning, China. *IOP Conf. Ser. Earth Environ. Sci.* **2020**, *558*, 032010. [[CrossRef](#)]
44. Kuang, H.; Bai, H.; Peng, N.; Qi, K.; Wang, Y.; Chen, X.; Liu, Y. Temporal and spatial distribution of Precambrian red beds and their formation mechanisms. *Geosyst. Geoenviron.* **2022**, *1*, 100098. [[CrossRef](#)]

Disclaimer/Publisher’s Note: The statements, opinions and data contained in all publications are solely those of the individual author(s) and contributor(s) and not of MDPI and/or the editor(s). MDPI and/or the editor(s) disclaim responsibility for any injury to people or property resulting from any ideas, methods, instructions or products referred to in the content.